Composite front maps for improved visibility of dynamic sea-surface features on cloudy SeaWiFS and AVHRR data

Peter Miller

Remote Sensing Group, Plymouth Marine Laboratory,
Prospect Place, Plymouth PL1 3DH, UK.

Abstract

Novel techniques have been developed for increasing the value of cloud-affected sequences of Advanced Very High Resolution Radiometer (AVHRR) sea-surface temperature (SST) data and Sea-viewing Wide Field-of-view Sensor (SeaWiFS) ocean colour data for visualising dynamic physical and biological oceanic processes such as fronts, eddies and blooms. The proposed composite front map approach is to combine the location, strength and persistence of all fronts observed over several days into a single map, which allows intuitive interpretation of mesoscale structures. This method achieves a synoptic view without blurring dynamic features, an inherent problem with conventional time-averaging compositing methods. Objective validation confirms a significant improvement in feature visibility on composite maps compared to individual front maps. A further novel aspect is the automated detection of ocean colour fronts, correctly locating 96% of chlorophyll fronts in a test data set. A sizeable data set of 13,000 AVHRR and 1,200 SeaWiFS scenes automatically processed using this technique is applied to the study of dynamic processes off the Iberian Peninsula such as mesoscale eddy generation, and many additional applications are identified. Front map animations provide a unique insight into the evolution of upwelling and eddies.

Keywords: Oceanic fronts; Mesoscale features; Geosensing; Infrared imagery; Water colour.

Article info: Miller, P.I. (2009) Composite front maps for improved visibility of dynamic sea-surface features on cloudy SeaWiFS and AVHRR data. Journal of Marine Systems, 78(3), 327-336. doi:10.1016/j.jmarsys.2008.11.019. This document is the author's post-print.

1 Introduction

The polar-orbiting AVHRR and SeaWiFS sensors provide frequent views of a wide range of physical and biological processes occurring at the sea surface, including: fronts, mesoscale eddies, currents, upwelling, phytoplankton and toxic algae blooms. Remote sensing of the marine environment is an established field, exploiting satellite data to study the development and distribution of oceanic processes (e.g. Haynes et al., 1993; Peckinpaugh and Holyer, 1994), and their effect on fisheries, sea mammals, ocean margin exchange and global warming (e.g. Huthnance, 1995; Podesta et al., 1993; Bost and others, this issue;). Oceanic fronts are formed at the boundary between water masses of different temperature or density, and are often associated with mixing and enhanced biological production. Fronts that extend to the sea surface may be observed by satellite if the water masses differ in temperature or colour. Identifying fronts in satellite images manually is a tedious and subjective task, so several researchers have proposed image processing algorithms to do this semi-automatically (e.g. Bardey et al., 1999; Simpson, 1990), or entirely automatically (Cayula and Cornillon, 1992). Tracking thermal features through a time-sequence of images allows sea-surface currents to be estimated (Breaker et al., 1994).

1.1 Compositing techniques

Oceanographic applications of visible and infrared satellite data are severely restricted by cloud cover, a limitation compositing techniques attempt to overcome by combining all cloud-free data

obtained from successive orbits. Assuming the weather system maintains regular movement of cloud across the region, over sufficient time a clear view of the ocean is achieved. The required time period may be a few days or more than a month depending on the cloudiness of the region. Conventional compositing methods average all cloud-free values obtained for each location, to produce a coarse distribution of temperature or chlorophyll (Feldman et al., 1989; Vazquez et al., 1994). These are of little value for analysing mesoscale features, because any dynamic aspects will be blurred in the time-averaged composite. Also, if half of a region is clear at the start of the compositing period and the other half is clear at the end, then any underlying change in temperature or chlorophyll during that time will produce an artificial front separating the two halves, which will confuse interpretation of any genuine features.

A few authors have combined the concepts of compositing and feature detection, by superimposing the locations of all fronts detected on a sequence of images to produce a single combined map. Clusters of fronts observed at different times near the same location indicate persistent oceanic features. Such techniques have been used to investigate the abundance of swordfish in relation to fronts (Podesta et al., 1993); to describe the seasonal distribution of fronts in the Baltic Sea (Kahru et al., 1995) and off the northeast US coast (Ullman and Cornillon, 1999); and to compile a visual database of manually identified mesoscale features in the Bay of Biscay (Bardey et al., 1999). Cayula and Cornillon improved the accuracy of automated front detection by incorporating evidence on persistent features derived from neighbouring days' images (Cayula and Cornillon, 1995).

1.2 Novel aspects of this study

The focus of this study is to increase the value of cloud-affected satellite data for visualising dynamic oceanic processes. Conventional composite methods calculate a time-averaged SST map and so blur dynamic features, while previous literature on combining fronts has examined static or recurring structures using weeks or months of imagery at a time. The proposed composite front map approach is to combine the location of all fronts observed over just a few days into a single map. Information on both the strength and persistence of those fronts is integrated in a unique visualisation that allows intuitive interpretation of the important oceanic processes. The dynamic development of these processes may be followed using animations of front map sequences, which overcome the problems of inadequate contrast and cloud flicker experienced using simple image animations. Other novel aspects include the automated detection of ocean colour fronts and biological processes using SeaWiFS data, and robust detection of very weak fronts using low-noise SST data.

2 Thermal front detection

The composite front map technique introduced in this paper initially requires the fronts to be detected on each individual satellite image. A review of previous work on thermal front detection (e.g. Holland and Yan, 1992; Holyer and Peckinpaugh, 1989; Simpson, 1990) identified the single-image edge detection (SIED) algorithm proposed by Cayula and Cornillon (1992) as the most promising approach for this task. SIED indicates fronts where there is a significant difference between the mean temperature of neighbouring water masses: this is a robust and completely automated method for distinguishing genuine oceanic fronts from numerous other thermal gradients on SST images. Cayula's validation using 98 satellite and in situ observations of the Gulf Stream front revealed the detection accuracy to be close to that of a human analyst. The technique has also been successfully applied to frontal analysis in other regions (Hickox et al., 2000; Kahru et al., 1995; Podesta et al., 1993; Ullman and Cornillon, 2001).

SIED only indicates a front where the mean temperatures of the adjacent water masses differ by at least 0.4 K, to limit false detections caused by sensor noise inherent in standard SST fields. Using low-noise SST data (see Appendix A) this difference may be reduced to 0.2 K, allowing detection of weaker fronts and more subtle oceanic structures close to the limit of AVHRR thermal sensitivity, which is approximately 0.1 K. This modification was found to significantly improve feature detection, as surface mixing often weakens the SST signal of strong fronts.

3 Ocean colour front detection

Although there exist a number of publications on remotely detecting thermal fronts, there has been limited investigation of automated detection of ocean colour fronts: for combining thermal and colour fronts in a single map to assess biophysical interactions (Miller, 2004); and for delineating water masses of differing bio-optical properties (Bontempi and Yoder, 2004; Belkin and O'Reilly, this issue). This paper validates the SIED method on SeaWiFS ocean colour products and demonstrates how composite front maps increase the value of partially cloudy ocean colour data for studying dynamic biological processes occurring at the sea-surface such as phytoplankton blooms. Also, SeaWiFS can reveal physical structure in greater detail than AVHRR due to the movement of phytoplankton pigment as a tracer.

Both SIED and the front compositing techniques are applicable to ocean colour data, though consideration should be given to a number of issues. Cloud-masking for SeaWiFS is currently not as effective as for AVHRR: there often remains a rim of pixels around the edge of clouds showing random high and low values, which may cause false front detections. A further issue is that certain SeaWiFS products such as chlorophyll-a are stored using log scaling. Although it is reasonable to derive fronts from log-scaled data, the resulting frontal gradients are variable across the data range, e.g. a value of 4 could represent any chlorophyll gradient from 0.02 mg m^{-3} km^{-1} at low concentrations to over 1 mg m^{-3} km^{-1} at high concentrations.

The most important consideration is the choice of SeaWiFS product from which to derive ocean colour fronts. Fronts extracted from each product will delineate different structures of the surface water depending on the radiance channel or channels used, so the choice depends upon the type of water constituent to be studied. For instance, the turbidity front associated with river plumes or coastal erosion could be studied using a suspended particulate matter (SPM) estimate derived from water leaving radiance at 555 or 670 nm, whereas the interaction of an eastern-boundary current with a phytoplankton-rich upwelling region would be best studied using the chlorophyll-a product. For certain applications it may be appropriate to produce front maps from all available wavelengths in order to visualise every structure present. The results in this paper concentrate on chlorophyll-a fronts, though similar front maps could have been derived from other SeaWiFS products.

4 Composite front map techniques

Applying SIED to a typical satellite image reveals only fragments of fronts observed through the gaps in cloud cover. The composite front map approach combines the locations of frontal fragments derived from all clear sea patches in a sequence of satellite images, to produce a synoptic view of dynamic ocean features. The compositing duration should be long enough to provide multiple observations of most genuine features, allowing them to be distinguished from artefacts, but not so long that features are obscured by multiple adjacent observations. This decision depends on the cloudiness of the region and frequency of satellite passes; the technique works best with multiple scenes each day. Three-day thermal front maps have been found to be appropriate for typically cloudy European waters, or 5-day for SeaWiFS chlorophyll maps.

A front map covering more than one day cannot be regarded as a snapshot of the region, but rather as a time-lapse picture showing a series of locations for the same dynamic features. Unlike conventional SST composites these dynamic features are not blurred and the full resolution can be retained for detailed analysis. The short-period composites used here are in contrast to previous work on combining fronts, which examined static rather than dynamic features using weeks or months of imagery at a time (e.g. Ullman and Cornillon, 1999).

Figure 1 provides a visual explanation of the creation of the composite front map, and also suggests that the resulting map achieves greater visibility of mesoscale oceanic features than any of the individual satellite images on their own. A quantitative validation of this hypothesis is provided in section 5.3.

4.1 Average front gradient

In order to create a composite front map it must be decided how the front segments detected on the sequence of individual images are to be combined. The simplest method would be to take the mean gradient magnitude from all fronts observed at the same pixel, ignoring any cloudy or non-front observations:

$$|\nabla(x, y, s)| = \begin{cases} \left[\left(\frac{\partial T(s)}{\partial x} \right)^2 + \left(\frac{\partial T(s)}{\partial y} \right)^2 \right]^{1/2}, & \text{if } (x, y) \in \mathbf{C}(s); \quad \text{for } s \in \{1,..,S\}, (x, y) \in \mathbf{I} \\ 0, & \text{if } (x, y) \notin \mathbf{C}(s) \end{cases}$$

$$F_{mean}(x, y) = \frac{\sum_{s=1}^{S} |\nabla(x, y, s)|}{|\{s, \text{such that } (x, y) \in \mathbf{C}(s)\}|}, \quad \text{for } (x, y) \in \mathbf{I}$$

T(s) is one SST (or chlorophyll) map in a sequence of S scenes. $|\nabla(x,y,s)|$ is the gradient magnitude of the corresponding set of SIED front contour pixels **C**(s), in degrees Kelvin per pixel distance (approx. K km^{-1}). F_{mean} is the mean composite front map derived from the sequence of S front maps. **I** is the set of valid image coordinates. The notation $|\{\ldots\}|$ means the number of elements in a set, so the divisor of the total magnitude is the number of scenes containing a front contour for that pixel.

4.2 Weighting by persistence and cloudiness

Although this simple method provides a direct estimate of the frontal gradient, it is flawed because it gives no greater weight to persistent fronts that are observed repeatedly at the same location. The front maps therefore appear cluttered by transient or noisy segments detected on only one scene in the sequence, making it difficult to recognise the persistent fronts delineating genuine features. Neither does it take any account of the varying cloudiness across the region: each cloud-free view devoid of fronts decreases the significance of any front previously detected in that region.

Persistence can be quantified as the probability of observing a front at a particular pixel during the sequence, P_{front}, calculated as the fraction of clear scenes that indicate fronts. A new formulation for the front map takes this into account by weighting the mean gradient by the persistence:

$$P_{front}(x, y) = \frac{|\{s, \text{such that } (x, y) \in \mathbf{C}(s)\}|}{|\{s, \text{such that } T(x, y, s) \neq t_{cloud}\}|}, \quad \text{for } (x, y) \in \mathbf{I}$$

$$F_{persist} = F_{mean} \, P_{front}$$

The constant t_{cloud} represents the distinct value assigned to cloudy pixels in the SST map. This new composite value $F_{persist}$ is defined both by the gradient and the frequency a front is observed at the same location, giving a strong visual cue to assist in interpretation. Unfortunately this makes it impossible to read the gradient magnitude directly off the image, as a pixel crossed by a strong front once may appear as bright as a pixel crossed by a weak front twice.

4.3 Weighting by neighbouring observations

The final enhancement explored is to incorporate prior knowledge that persistent features may be displaced during the compositing time period due to advection, tides, or residual geocorrection errors. To highlight such features it is necessary to consider the spatial proximity of front contours in one scene to those in other scenes. F_{nhood} determines the extent and weighting of the neighbourhood to consider around each front, and is calculated by convolution of an individual front map with a Gaussian smoothing filter of width σ=2 pixels (2.2 km) and a peak value of 1.0. Each contour location on one front map is examined in all other F_{nhood} scenes to calculate F_{other}, the mean of any indications that those locations are in proximity to further contours:

$$F_{other}(x, y, r) = \frac{\sum_{s=1, s\neq r}^{S} F_{nhood}(x, y, s)}{\left|\{s, \text{such that } s \neq r, F_{nhood}(x, y, s) > 0\}\right|}, \quad \text{for } r \in \{1,.., S\}, (x, y) \in \mathbf{C}(r)$$

$$F_{prox}(x, y) = \frac{\sum_{s=1}^{S} F_{other}(x, y, s)}{\left|\{s, \text{such that } F_{other}(x, y, s) > 0\}\right|}, \quad \text{for } (x, y) \in \mathbf{I}$$

$$F_{comp} = F_{mean}\ P_{front}\ F_{prox}$$

A minimum value of 0.25 is assigned to all F_{other} contours, to ensure that even those without close neighbours appear in the final front map. F_{prox} is the mean of all the F_{other} maps, summarising the evidence that any particular location is in close proximity to a persistent feature. The composite front map is weighted by the proximity map to incorporate this information in the visualisation.

5 Validation of front detection techniques

5.1 Truth data

The accuracy of automated front detection must be assessed by comparison with the true locations of fronts. This would be obtained ideally through analysis of in situ transects of chlorophyll and temperature measurements, though insufficient quantities of suitable data were available for this project. Instead, remote sensing 'truth' data were obtained in the form of manual annotations of the front locations provided by a remote sensing analyst. This is a difficult and subjective task, as remotely sensed fronts are generally seen as smooth gradients rather than step edges. Therefore the analyst was asked only to delineate the offshore boundary of the upwelling zone on summer images of the NW Iberian Peninsula, as this is usually a significant front. In total 97 AVHRR SST images and 43 SeaWiFS chlorophyll images from June to September 1998 were used for validation, from which respectively 7 and 10 predominantly cloud-free scene were manually annotated with the 'true' upwelling front. The remainder from neighbouring days were used to test whether the composite front map approach improved the visibility of the true front using cloudy imagery.

Testing was performed objectively by plotting short segments approximately normal to the true front contour, and analysing pixel locations along each segment in the automatic front maps to calculate the shortest distance between the true front and a detected front (Figure 2). Approximately 30 segments were placed on each contour, totalling 209 and 200 locations to validate for front detection on SST and chlorophyll respectively. The metrics used in validation are defined as follows: hit rate - the percentage of segments that cross detected fronts; offset - the distance in pixels from the true front to the closest crossing of a detected front; false alarms - the number of additional crossings of detected fronts. False alarms are often overlooked in rating general detection performance, but can be as important as the hit rate. In an extreme case where the automatic method indicated fronts at every pixel on the image, the 100% hit rate and 0 offset would be misleading without a measurement of false alarms. As the segments extend 10 pixels in both directions, there can be at most 1 hit and 20 false alarms.

5.2 Front detection on individual images

Validation of the SIED front detection algorithm on individual images has previously been performed comprehensively by the originators of this technique, who found the accuracy to be close to that of a trained analyst (Cayula and Cornillon, 1992). However, additional testing on this different geographical area is still valuable to confirm the generality of this algorithm. Table 1 summarises the results of front detection on the 14 images annotated by the human analyst. On average, 93% of the thermal fronts were detected, with an offset of approximately 2 pixels (2.2 km) from the true front and 1.5 false alarms; and 94% of the chlorophyll fronts were detected, with an offset of 2.3 pixels (2.5 km) and 2 false alarms. These results indicate accurate and robust detection of the genuine fronts on

both SST and, for the first time, on chlorophyll data, and provide good justification for the use of SIED as the basis for the novel compositing techniques validated in the following section.

5.3 Composite front map detection

The new technique for producing composite front maps involves combining front locations detected on a short sequence of cloudy individual images. Front maps were generated using all individual SST data acquired within the 3-day window centred on the date of each truth image, and a wider 5-day window for chlorophyll data due to the less frequent coverage of SeaWiFS. It is important to note that the exceptionally cloud-free truth images were excluded from the composite in order to test the method on data with typical cloud-cover. This left approximately 15 SST and 3 chlorophyll scenes in the time-window for each truth image. The cloudiness of each data set was quantified as the mean percentage of the true front that could be observed using an individual scene. The aim was to evaluate any improvement in feature visibility of these short-period front maps compared to individual scenes: F_{comp} or the simple F_{mean} map could be used equally as the additional visual cues provided by the F_{comp} metric were not considered in this analysis.

The improved visibility of the true front afforded by composite front maps is striking (Table 2). Whereas only 34% of the true front was visible in an individual SST scene, the single composite map detected 94%. The composite chlorophyll front maps detected 96% of the true front, compared to 68% visibility on the individual scenes. The original chlorophyll scenes are less cloudy than SST because SeaWiFS data are acquired near local noon, which is generally the least cloudy time of day in this region. The composite front map also achieved good positional accuracy: a small offset of 1.2 pixels (1.3 km) from the true thermal fronts, though the multiple superimposed contours resulted in a high false alarm rate (6.3): these are normally seen as a cluster of alternate locations of the real front rather than false front locations. The composite chlorophyll front map achieved 1.8 pixel (2.0 km) offset and 4.7 false alarms.

Figure 3 shows an example chlorophyll front map for the UK Western Approaches derived from all SeaWiFS data acquired 16-22 Jul. 2000. The F_{comp} map is presented as a simple grey-scale, with darker greys indicating stronger or more persistent fronts. This allows intuitive interpretation of the important oceanic processes: enhanced productivity along the tidal front between the Irish and Celtic Seas, and three large phytoplankton blooms near Ireland and Cornwall. The bloom south of Cornwall when sampled in situ showed extremely high concentrations (10,000 cells ml^{-1}) of the dinoflagellate Karenia mikimotoi (Groom et al., 2000).

6 Analysis of Iberian Peninsula dynamics

This section aims to demonstrate the benefit of composite front maps in the study of dynamic processes using a case study off the Atlantic Coast of the Iberian Peninsula (Figure 4). In the summer this region is dominated by northerly winds favourable to upwelling, causing dynamic physical and biological changes at the sea-surface of considerable importance to ocean margin exchange (Huthnance, 1995) and fisheries (Tenore et al., 1995). Topographic forcing or frontal instabilities cause transient cold water filaments to extend up to 200 km from the upwelling zone into the deeper ocean (Haynes et al., 1993). Mesoscale eddies may form along the continental slope and influence local circulation and mixing; if they detach as a slope-water oceanic eddy (Swoddy) they can transport their physical properties over thousands of kilometres and many months (Pingree and Lecann, 1992).

In order to study the spatial and temporal distribution of these dynamic processes a huge satellite data set was acquired, calibrated and geolocated: 13,000 AVHRR images between 1993 and 2000, and 1200 SeaWiFS images since launch in September 1997. The procedure for converting AVHRR and SeaWiFS raw satellite data into calibrated ocean temperature and colour products is summarised in Appendix A. Composite front maps were processed automatically for the entire data set, confirming the robustness of the technique. Only SST front maps are shown as the significant processes are most clearly visualised by their thermal signature. Due to the sensitivity of front detection and enhancement of persistent features, animations of upwelling periods reveal unparalleled detail of the turbulent currents associated with filaments and eddies. A 'rolling' scheme is employed for animations so that

each frame changes by adding only one new day and removing one old day of data. Cloud-covered regions show previously detected fronts until new fronts are detected, though if cloud persists for longer than a week a warning is given that the situation may have since changed by turning the background colour of that region increasingly yellow like old paper. As only sample frames can be included here, readers are encouraged to view the full animations on the web site: http://www.npm.ac.uk/papers/miller_jms2008/.

The SST front map for 3-5 Aug. 1998 delineates the upwelling zone and four filaments indicated by offshore arrows (Figure 5a). The concave front between the upper two filaments results from the intrusion of a warm jet flowing south-east into the upwelled waters, mixing by way of a cyclonic-anticyclonic pair of eddies (Smyth et al., 2001). Two weeks later the dynamic growth of a new filament is captured, originating from Cape Finisterre (Figure 5b). Manual tracking of the 'nose' of the filament was used to estimate a growth rate of 13 cm s^{-1}, though it was determined in situ using ADCP that this growth is supported by a stronger offshore current within the filament of 28 cm s^{-1} at 25 m depth (Smyth et al., 2001). The mature filament further south has become entrained around the same anticyclonic eddy marked in Figure 5a.

The Galician region is subject to frequent mesoscale eddies at depth, and occasionally their thermal signature becomes visible at the sea-surface (Figure 6a). The eddies indicated to the west of Iberia appear to be topographically generated as their locations coincide with the seamounts seen in Figure 4; other eddies result from interactions between Mediterranean and Atlantic water masses. Favourable meteorological conditions allowed the rotation, advection and distortion of these eddies to be followed for ten days by manually tracking persistent features on their boundaries (Figure 6b).

At depths greater than 600 m, the Iberian coast is characterised by the poleward flow of Mediterranean Intermediate Water, though during the summer upwelling season the surface pattern is equatorward. In the absence of upwelling winds in winter the poleward flow often reaches the surface where it can be studied by satellite (Haynes and Barton, 1990). The front map for 16-18 Jan. 1996 shows anomalously warm surface water extending past the North coast of Spain into the Bay of Biscay (Figure 7a). This front map is overlaid on a greyscale composite of SST data from the same period to highlight the currents; the scale of F_{comp} is reversed with white lines indicating more significant fronts. (This form of presentation is not always helpful as conventional composites are subject to patchy artefacts that obscure subtle front contours.) The interaction between the poleward current and slope water can lead to the generation of eddies at capes such Cabo Roca near Lisbon. A sequence from Nov. 1999 depicts in detail the surface signature of a cyclonic eddy detaching from the coast (Figure 7b): this event may be associated with the generation of an anticyclonic Swoddy in adjacent water (Pingree and Lecann, 1993).

7 Discussion

This new methodology for processing satellite data has been shown by example and quantitative validation to improve the visibility of dynamic oceanic processes. It is applicable to any geographic area and any type of satellite ocean colour or temperature product; it is also robust and can be completely automated. The remaining problems are concerned with performance on predominantly cloudy sequences. The regional-statistical approach of SIED appears to impose a limit on the smallest cloud-free patch that may be used to extract a front contour, so even a 7-day composite may present very few fronts in cloudy regions. It is hoped this problem may be tackled by automatically reducing the window size and strictness of statistical criteria in cloud-affected parts of a scene (e.g. Diehl et al., 2002). Also, in cloudy regions it is not known a priori the composite duration required to provide multiple observations of persistent features, and so the resulting front maps are often degraded by transient contours. A practical solution would be to continue to composite additional days until each region has acquired a certain density of front detections. This may also counter the inverse problem, of too many observations causing large clusters of parallel contours that obscure neighbouring features.

The front detection algorithm performs equally well on SST and chlorophyll data, though visualisation of dynamic processes is limited by the repeat rate of only one SeaWiFS pass each day.

The adaptive duration already proposed may improve results, and the proximity test should be modified to recognise larger displacements between successive observations. The techniques are now being extended to combine front data from multiple AVHRR and SeaWiFS products in a single map, to explore the interactions between physical and biological processes.

Many potential applications have been recognised, some of which are being developed with collaborators: data reduction, for quickly finding features of interest in many months of data; fisheries management, by providing better information on environmental factors affecting their distribution; studies of meandering currents and eddy formation; hydrodynamic model validation; evolution of phytoplankton and harmful algae blooms and sediment plumes from river outflows or coastal erosion; data compression for microsatellite storage and downlinks; and feature tracking, which would become more tractable based on the detected water mass boundaries. These techniques should also be complementary to other modalities such as altimetry, for example to provide greater spatial and temporal resolution on the dynamics of certain eddies observed in both datasets.

8 Conclusions

A novel compositing method has been shown to significantly improve the visibility of mesoscale oceanic features in cloudy regions, by automatically combining frontal information from a sequence of satellite data. In addition to AVHRR SST fronts, the method has been validated on SeaWiFS chlorophyll fronts and is equally applicable to other ocean colour products for visualising biological processes such as algae blooms. Advanced compositing methods have been described and validated in terms of their sensitivity, accuracy and robustness, meeting the requirements for many potential applications. Animations reveal new insights into the dynamic nature of upwelling and eddies.

Acknowledgements

I would like to thank the other members of the PML Remote Sensing Group for their assistance and suggestions on this research, NASA SeaWiFS Project and Orbimage for SeaWiFS data, NERC Dundee Receiving Station for acquisition of all satellite data, Jean-Francois Cayula for assistance in implementation of SIED, and five reviewers for constructive comments. This research formed part of the PML Core Strategic Research Programme, and was partially funded by QinetiQ, Space Department, Farnborough, UK.

Appendix A. Processing AVHRR and SeaWiFS satellite data

The Plymouth Marine Laboratory Remote Sensing Group (RSG) has over a number of years developed an automated system for processing large quantities of satellite data from the AVHRR and SeaWiFS instruments (Miller et al., 1997). This system, called Panorama, is run continuously to process the data into calibrated ocean temperature and colour products within two hours of the satellite overpass. A prerequisite of the front detection methods is a long time-series of calibrated, cloud-masked and accurately navigated satellite data. Ideally several images should be acquired for the same area each day to reduce the compositing period necessary to achieve synoptic views and increase the available information on front persistence. RSG acquires 8-9 AVHRR passes every day, providing up to 4 views of most regions within receiving range. SeaWiFS coverage is limited to 2-3 passes over each receiving station every day, giving at most a single view of any area.

Panorama incorporates several improvements over standard AVHRR processing schemes that benefit front detection. First, an automated navigation adjustment scheme matches a database of pre-defined ground control points such as islands or headlands with image features found close to the locations predicted by the orbital model (Bordes et al., 1992).This enables long image sequences to be processed without manual navigation correction. The cloud-masking procedure is a hybrid of a number of novel and standard techniques based on the temperature, reflectance and texture of the AVHRR scene, and has been shown by objective testing to be superior to established methods (e.g. Saunders and Kriebel, 1988). The effect of this is to reduce false front detections caused by cloud contamination of SST data. Finally, the Partial SST technique developed for Panorama applies a 2D

smoothing filter to the atmospheric correction component of the SST equation, considerably reducing noise in the temperature estimates without blurring oceanic structures (Miller et al., 1997).

SeaWiFS processing in Panorama is based on NASA SeaDAS routines (NASA, 2007), but incorporates an atmospheric correction algorithm for sediment-dominated coastal waters (Moore et al., 1999). Further details on the processing scheme can be found in Lavender and Groom (1999). The set of oceanic parameters derived from each SeaWiFS pass includes: normalised water-leaving radiance (L_{wn}) at 412, 443, 490, 510, 555 nm; chlorophyll-a concentration; diffuse attenuation coefficient (K_d 490); and true-colour composite.

9 References

Bardey, P., Garnesson, P., Moussu, G. and Wald, L., 1999. Joint analysis of temperature and ocean colour satellite images for mesoscale activities in the Gulf of Biscay. International Journal of Remote Sensing, 20(7): 1329-1341.

Belkin, I.M. and O'Reilly, J.E., this issue. An algorithm for oceanic front detection in chlorophyll and sea surface temperature satellite imagery. Journal of Marine Systems.

Bontempi, P.S. and Yoder, J.A., 2004. Spatial variability in SeaWiFS imagery of the South Atlantic bight as evidenced by gradients (fronts) in chlorophyll a and water-leaving radiance. Deep-Sea Research Part II-Topical Studies in Oceanography, 51(10-11): 1019-1032.

Bordes, P., Brunel, P. and Marsouin, A., 1992. Automatic adjustment of AVHRR navigation. Journal of Atmospheric and Oceanic Technology, 9(1): 15-27.

Bost and others, this issue. Importance of Southern Ocean fronts for seabirds and sea mammals. Journal of Marine Systems.

Breaker, L.C., Krasnopolsky, V.M., Rao, D.B. and Yan, X.H., 1994. The feasibility of estimating ocean surface currents on an operational basis using satellite feature tracking methods. Bulletin of the American Meteorological Society, 75(11): 2085-2095.

Cayula, J.F. and Cornillon, P., 1992. Edge-detection algorithm for SST images. Journal of Atmospheric and Oceanic Technology, 9(1): 67-80.

Cayula, J.F. and Cornillon, P., 1995. Multi-image edge detection for SST images. Journal of Atmospheric and Oceanic Technology, 12(4): 821-829.

Diehl, S.F., Budd, J.W., Ullman, D. and Cayula, J.F., 2002. Geographic window sizes applied to remote sensing sea surface temperature front detection. Journal of Atmospheric and Oceanic Technology, 19(7): 1105-1113.

Feldman, G.C., Kuring, N.A., Ng, C. and et al., 1989. Ocean color: availability of the global data set. EOS, 70: 634-641.

Groom, S.B., Tarran, G.A. and Smyth, T.J., 2000. Red-tide outbreak in the English Channel, Backscatter, pp. 8-11 (Fall).

Haynes, R. and Barton, E.D., 1990. A poleward flow along the Atlantic Coast of the Iberian Peninsula. Journal of Geophysical Research-Oceans, 95(C7): 11425-11441.

Haynes, R., Barton, E.D. and Pilling, I., 1993. Development, persistence, and variability of upwelling filaments off the Atlantic Coast of the Iberian Peninsula. Journal of Geophysical Research-Oceans, 98(C12): 22681-22692.

Hickox, R., Belkin, I., Cornillon, P. and Shan, Z., 2000. Climatology and seasonal variability of ocean fronts in the east China, Yellow and Bohai Seas from satellite SST data. Geophysical Research Letters, 27(18): 2945-2948.

Holland, J.A. and Yan, X.H., 1992. Ocean thermal feature recognition, discrimination, and tracking using infrared satellite imagery. IEEE Trans. Geoscience and Remote Sensing, 30(4): 818-824.

Holyer, R.J. and Peckinpaugh, S.H., 1989. Edge detection applied to satellite imagery of the oceans. IEEE Trans. Geoscience and Remote Sensing, 27: 46-56.

Huthnance, J.M., 1995. Circulation, exchange and water masses at the ocean margin: the role of physical processes at the shelf edge. Progress in Oceanography, 35: 353-431.

Kahru, M., Hakansson, B. and Rud, O., 1995. Distributions of the sea-surface temperature fronts in the Baltic Sea as derived from satellite imagery. Continental Shelf Research, 15(6): 663-679.

Lavender, S.J. and Groom, S.B., 1999. The SeaWiFS automatic data processing system (SeaAPS). International Journal of Remote Sensing, 20(6): 1051-1056.

Miller, P., Groom, S., McManus, A., Selley, J. and Mironnet, N., 1997. Panorama: a semi-automated AVHRR and CZCS system for observation of coastal and ocean processes, RSS97: Observations and Interactions, Proceedings of the Remote Sensing Society, Reading, pp. 539-544.

Miller, P.I., 2004. Multispectral front maps for automatic detection of ocean colour features from SeaWiFS. International Journal of Remote Sensing, 25(7-8): 1437-1442.

Moore, G.F., Aiken, J. and Lavender, S.J., 1999. The atmospheric correction of water colour and the quantitative retrieval of suspended particulate matter in Case II waters: application to MERIS. International Journal of Remote Sensing, 20(9): 1713-1733.

NASA, 2007. SeaDAS web site. http://oceancolor.gsfc.nasa.gov/seadas/.

Peckinpaugh, S.H. and Holyer, R.J., 1994. Circle detection for extracting eddy size and position from satellite imagery of the ocean. IEEE Transactions on Geoscience and Remote Sensing, 32(2): 267-273.

Pingree, R.D. and Lecann, B., 1992. 3 anticyclonic slope water oceanic eddies (SWODDIES) in the Southern Bay of Biscay in 1990. Deep-Sea Research Part A, 39(7-8A): 1147-1175.

Pingree, R.D. and Lecann, B., 1993. A Shallow Meddy (a Smeddy) From the Secondary Mediterranean Salinity Maximum. Journal of Geophysical Research-Oceans, 98(C11): 20169-20185.

Podesta, G.P., Browder, J.A. and Hoey, J.J., 1993. Exploring the association between swordfish catch rates and thermal fronts on United-States longline grounds in the Western North-Atlantic. Continental Shelf Research, 13(2-3): 253-277.

Saunders, R.W. and Kriebel, K.T., 1988. An improved method for detecting clear sky and cloudy radiances from AVHRR data. International Journal of Remote Sensing, 9: 123-150.

Simpson, J.J., 1990. On the accurate detection and enhancement of oceanic features observed in satellite data. Remote Sensing of Environment, 33(1): 17-33.

Smyth, T.J., Miller, P.I., Groom, S.B. and Lavender, S.J., 2001. Remote sensing of sea surface temperature and chlorophyll during Lagrangian experiments at the Iberian margin. Progress in Oceanography, 51(2-4): 269-281.

Tenore, K.R. et al., 1995. Fisheries and oceanography off Galicia, NW Spain - mesoscale spatial and temporal changes in physical processes and resultant patterns of biological productivity. Journal of Geophysical Research-Oceans, 100(C6): 10943-10966.

Ullman, D.S. and Cornillon, P.C., 1999. Satellite-derived sea surface temperature fronts on the continental shelf off the northeast US coast. Journal of Geophysical Research-Oceans, 104(C10): 23459-23478.

Ullman, D.S. and Cornillon, P.C., 2001. Continental shelf surface thermal fronts in winter off the northeast US coast. Continental Shelf Research, 21(11-12): 1139-1156.

Vazquez, J., Hamilton, M., Van Tran, A. and Sumagausay, R., 1994. JPL Physical Oceanography DAAC reprocesses ten years of sea-surface temperature measurements from NOAA AVHRR. The Earth Observer, ESA, 6: 16-17.

Figure legends

Figure 1. Schematic diagram of new composite front map technique. 30 AVHRR SST maps (three shown) of the Irish shelf within a 7-day window are processed using the SIED algorithm to detect front locations, which are then composited to calculate the mean frontal gradient F_{mean}, the probability of detecting a front P_{front}, and the evidence for a feature in proximity F_{prox}. These weighting factors are combined as the composite front map F_{comp} to provide optimal visualisation of all oceanic features observed during the period.

Figure 2. Validation technique for front detection: (a) Example chlorophyll image overlaid in white with 'true' upwelling front contour and segments approximately normal to contour; (b) Corresponding front map overlaid with segments used to measure accuracy of front detection.

Figure 3. Chlorophyll composite front map 16-22 Jul. 2000 for UK Western Approaches, showing enhanced productivity along fronts and three phytoplankton blooms.

Figure 4. Map showing bathymetry of study area off NW Iberian Peninsula.

Figure 5. Upwelling and filaments at the NW Iberian Peninsula: (a) SST front map 3-5 Aug. 1998 with filaments, a warm jet and eddies indicated by arrows; (b) SST front maps for 17-19 and 22-24 Aug. 1998 showing dynamic growth of new filament.

Figure 6. Mesoscale eddies at the NW Iberian Peninsula: (a) SST front map 29-31 Mar. 1997 with several eddies indicated by arrows; (b) Sequence of SST front maps during Mar.-Apr. 1997 showing rotation, advection and distortion of two eddies, region indicated by rectangle in main figure.

Figure 7. Poleward flow at the NW Iberian Peninsula: (a) SST front map 16-18 Jan. 1996 showing winter poleward flow of warm water at the surface; (b) Sequence of SST front maps from Nov. 1999 showing a cyclonic eddy detaching from shelf-edge near Lisbon.

Tables

Table 1. Front detection performance on the truth images. The upper half of the table relates to SST images, and the lower half to chlorophyll images.

Truth image	Segments	Front hit rate (%)	Offset	False Alarms
29 Jul. 1998 1519	33	81.8	2.2	1.6
31 Jul. 1998 1457	16	93.8	1.6	1.1
03 Aug. 1998 1423	36	91.7	2.9	1.2
05 Aug. 1998 1542	42	92.9	1.7	2.1
10 Aug. 1998 1446	21	95.0	1.7	1.9
18 Aug. 1998 1458	27	96.2	1.3	0.8
21 Aug. 1998 0644	34	100.0	2.3	1.7
SST: mean ± S.D.	30	93.0±5.6	2.0±0.5	1.5±0.5
18 Jun. 1998 1318	15	100.0	1.0	2.3
19 Jul. 1998 1322	22	100.0	2.3	2.8
29 Jul. 1998 1229	27	96.3	1.9	2.6
03 Aug. 1998 1255	26	88.0	1.5	1.5
06 Aug. 1998 1330	23	78.3	4.7	0.8
12 Aug. 1998 1302	37	83.8	2.8	1.5
18 Aug. 1998 1235	32	96.9	2.6	1.8
21 Aug. 1998 1310	26	92.3	1.8	2.6
10 Sep. 1998 1317	15	100.0	2.0	1.9
18 Sep. 1998 1240	24	100.0	2.3	1.7
Chlor.: mean ± S.D.	25	93.6±7.8	2.3±1.0	2.0±0.6

Front detection performance on individual truth images. Upper and lower halves of the table relate to SST and chlorophyll data respectively. 'Segments' denotes the number of line segments placed across each true contour in order to validate the front detection at those locations.

Table 2. Front detection performance using composite front maps, comprising all fronts detected during the 3-day window (or 5-day window for chlorophyll) centred on date of truth image.

Truth image EXCLUDED from composite map	**Mean front visibility (%)**	**Composite front map hit rate (%)**	**Offset**	**False alarms**
29 Jul. 1998 1519	22.6	84.9	1.5	5.2
31 Jul. 1998 1457	33.6	100.0	1.1	7.2
03 Aug. 1998 1423	35.3	97.2	0.9	5.5
05 Aug. 1998 1542	55.7	100.0	0.7	10.0
10 Aug. 1998 1446	18.1	81.0	1.9	3.7
18 Aug. 1998 1458	35.0	96.3	1.1	5.9
21 Aug. 1998 0644	35.1	97.1	1.3	6.5
SST: mean ± S.D.	**33.6**±11.9	**93.8**±7.6	1.2±0.4	6.3±1.9
18 Jun. 1998 1318	84.4	100.0	1.1	5.7
19 Jul. 1998 1322	75.0	100.0	1.1	7.2
29 Jul. 1998 1229	71.3	96.3	1.3	6.2
03 Aug. 1998 1255	91.0	96.2	1.6	5.7
06 Aug. 1998 1330	71.7	100.0	1.0	5.0
12 Aug. 1998 1302	77.0	86.5	2.5	2.2
18 Aug. 1998 1235	47.9	96.9	3.3	1.8
21 Aug. 1998 1310	96.2	92.3	2.1	3.6
10 Sep. 1998 1317	36.7	86.7	2.7	3.2
18 Sep. 1998 1240	24.0	100.0	1.5	6.8
Chlor.: mean ± S.D.	**67.5**±24	**95.5**±5.3	1.8±0.8	4.7±1.9

Front detection performance using composite front maps comprising all fronts detected during the 3-day window (or 5-day window for chlorophyll) centred on date of truth image, but excluding the truth image itself. Composite front map hit rate is compared with the mean front visibility of an individual scene. Upper and lower halves of the table relate to SST and chlorophyll data respectively.

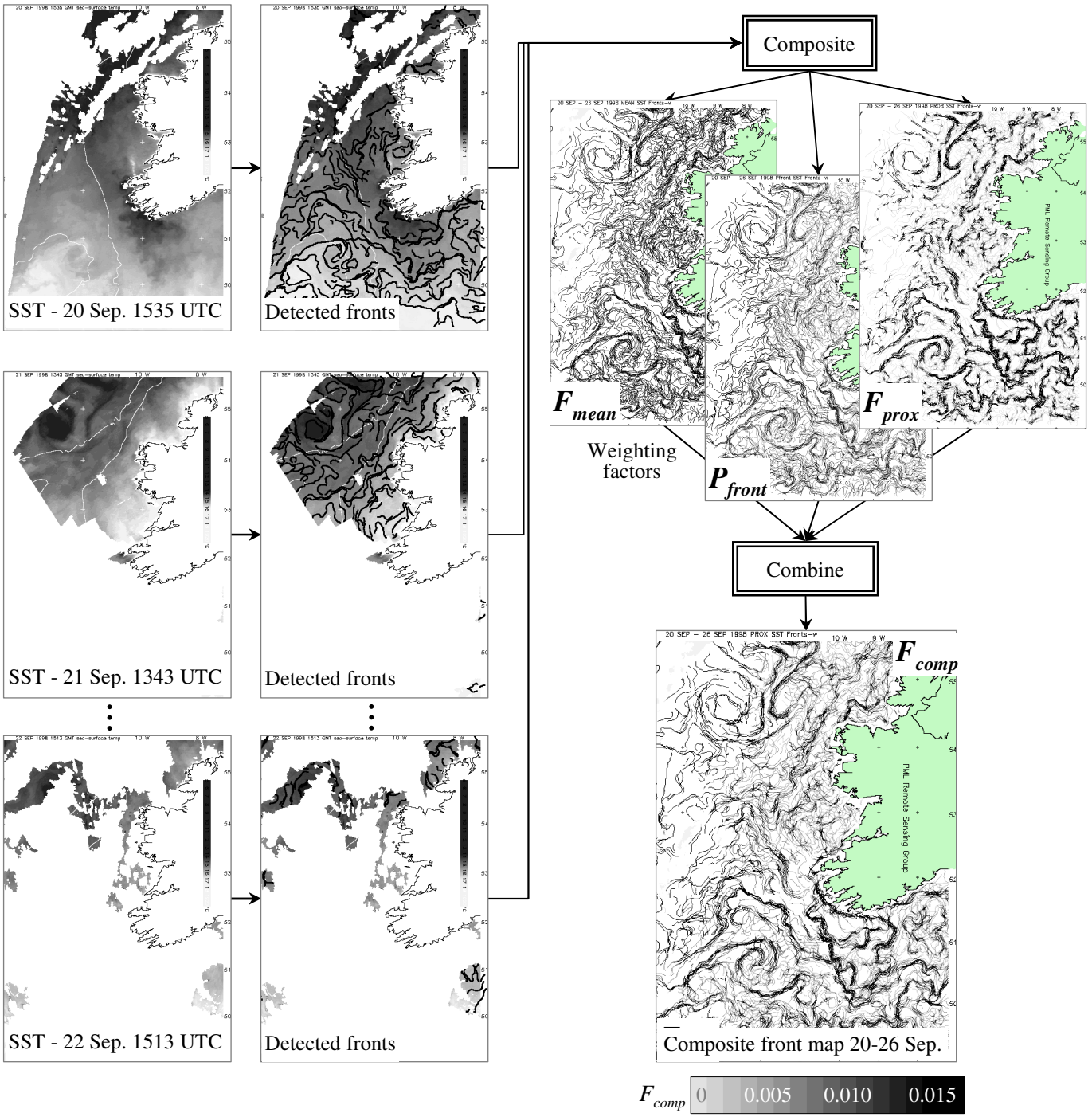

Figure 1. Schematic diagram of new composite front map technique. 30 AVHRR SST maps (three shown) of the Irish shelf within a 7-day window are processed using the SIED algorithm to detect front locations, which are then composited to calculate the mean frontal gradient F_{mean}, the probability of detecting a front P_{front}, and the evidence for a feature in proximity F_{prox}. These weighting factors are combined as the composite front map F_{comp} to provide optimal visualisation of all oceanic features observed during the period.

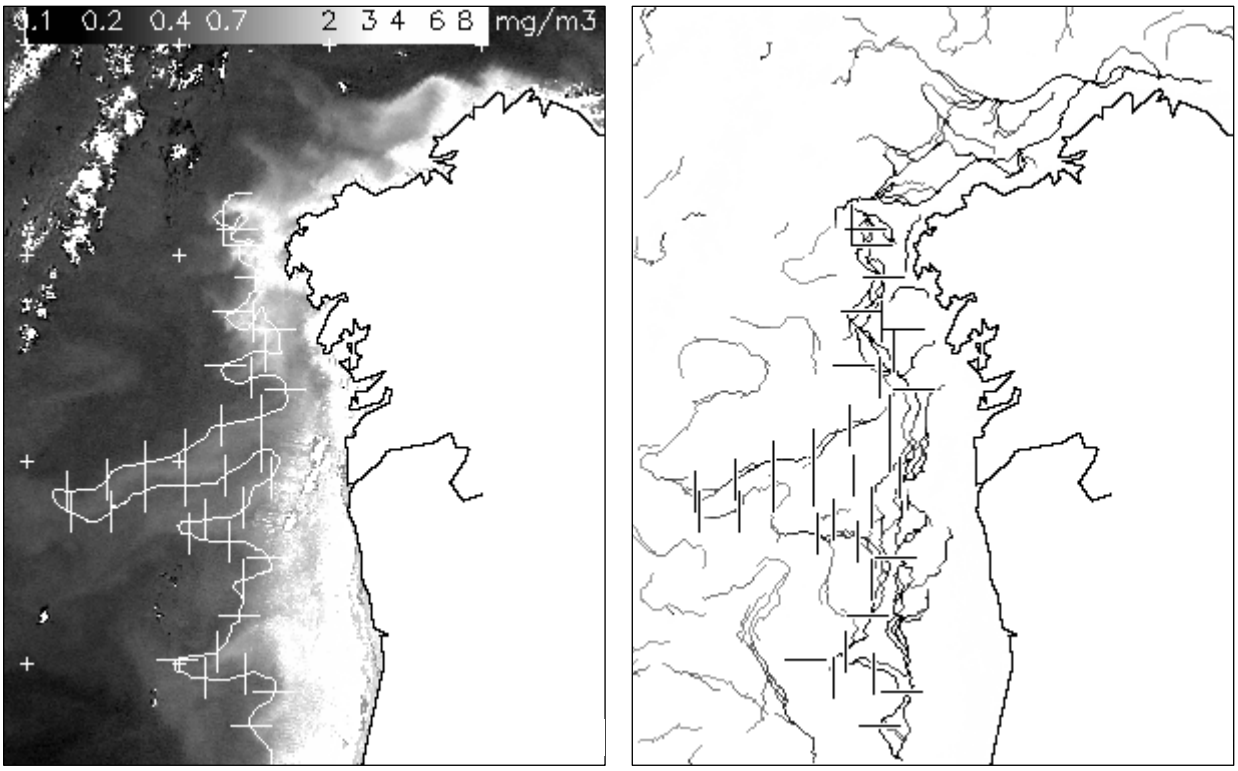

(a) *(b)*

Figure 2. Validation technique for front detection: (a) Example chlorophyll image overlaid in white with 'true' upwelling front contour and segments approximately normal to contour; (b) Corresponding front map overlaid with segments used to measure accuracy of front detection.

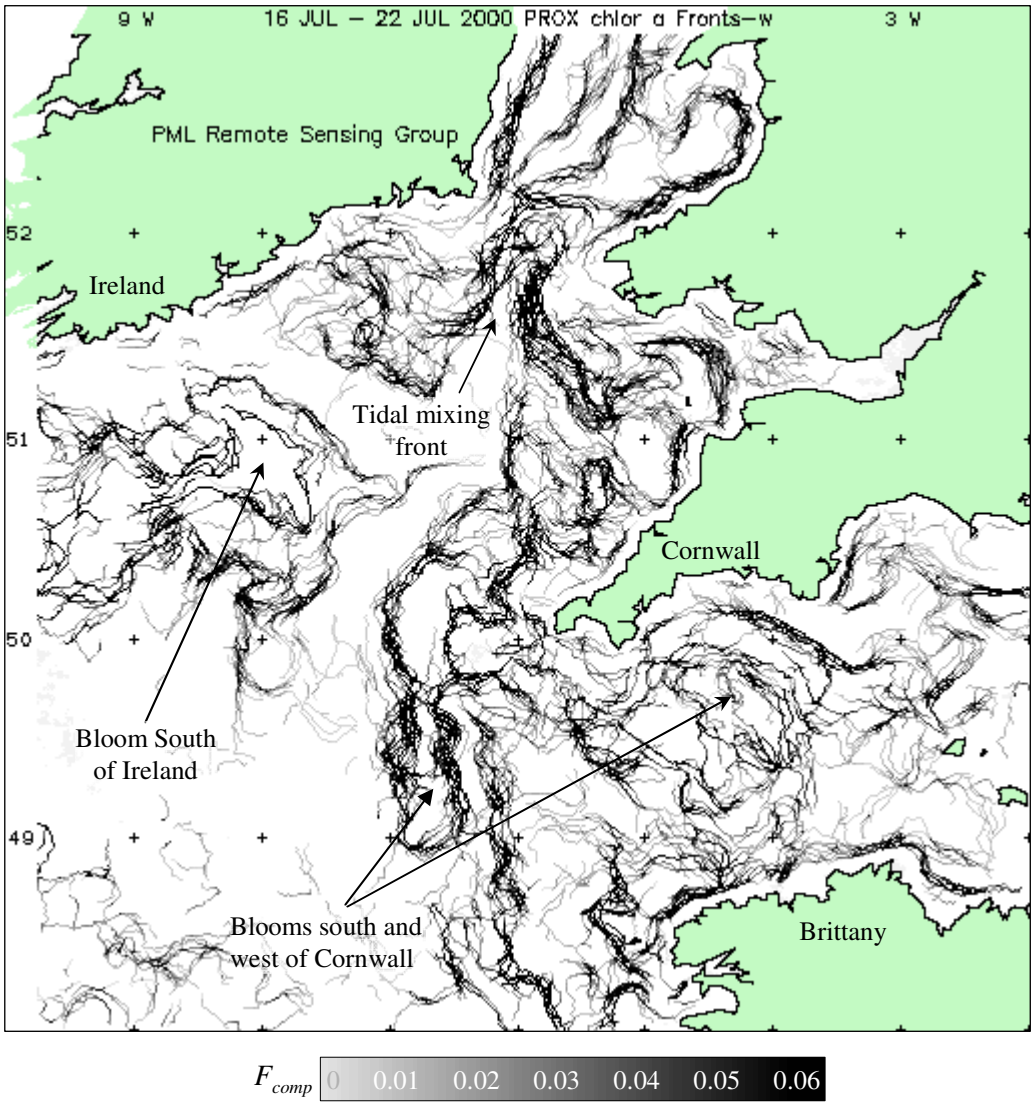

Figure 3. Chlorophyll composite front map 16-22 Jul. 2000 for UK Western Approaches, showing enhanced productivity along fronts and three phytoplankton blooms.

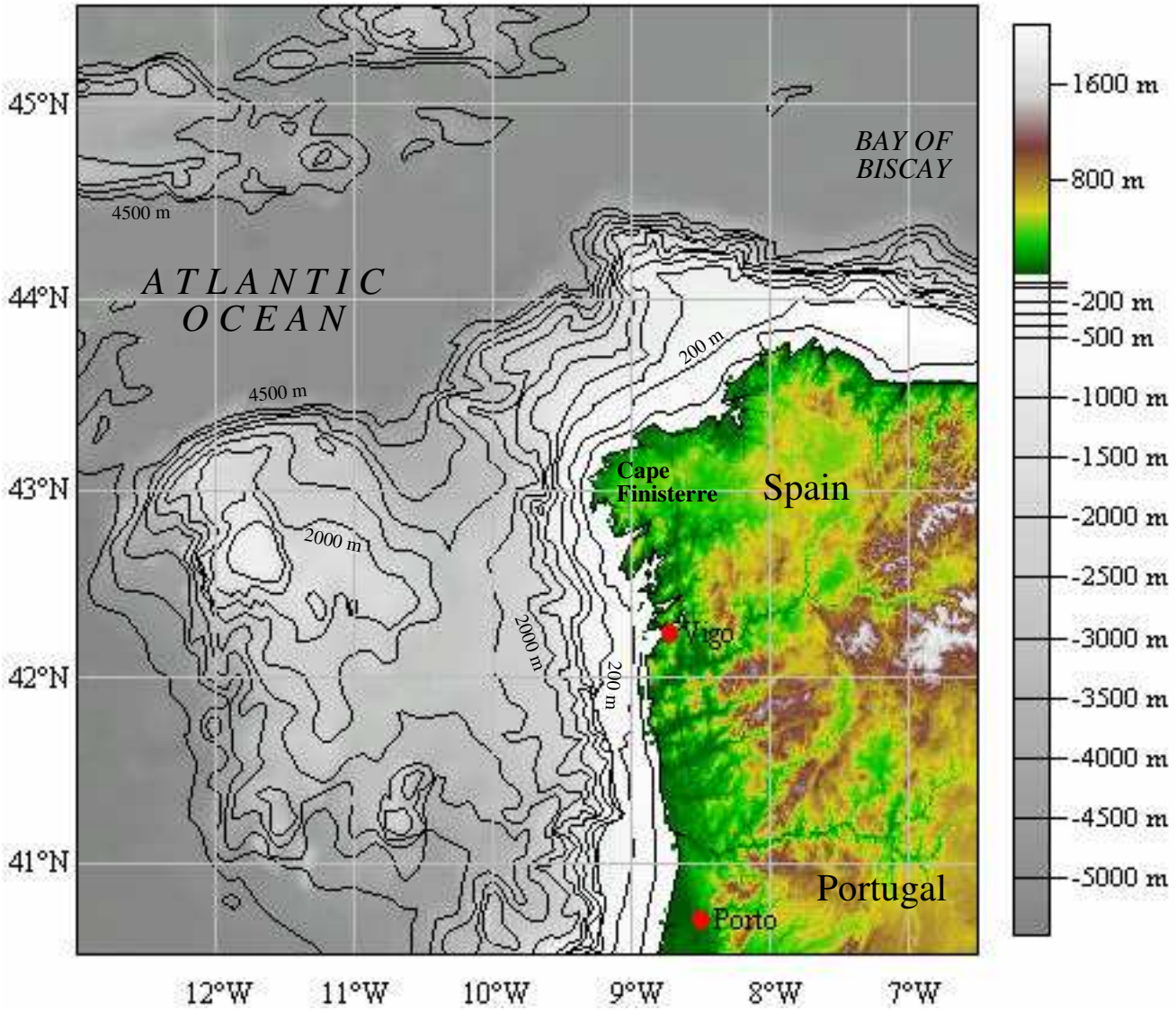

Figure 4. Map showing bathymetry of study area off NW Iberian Peninsula.

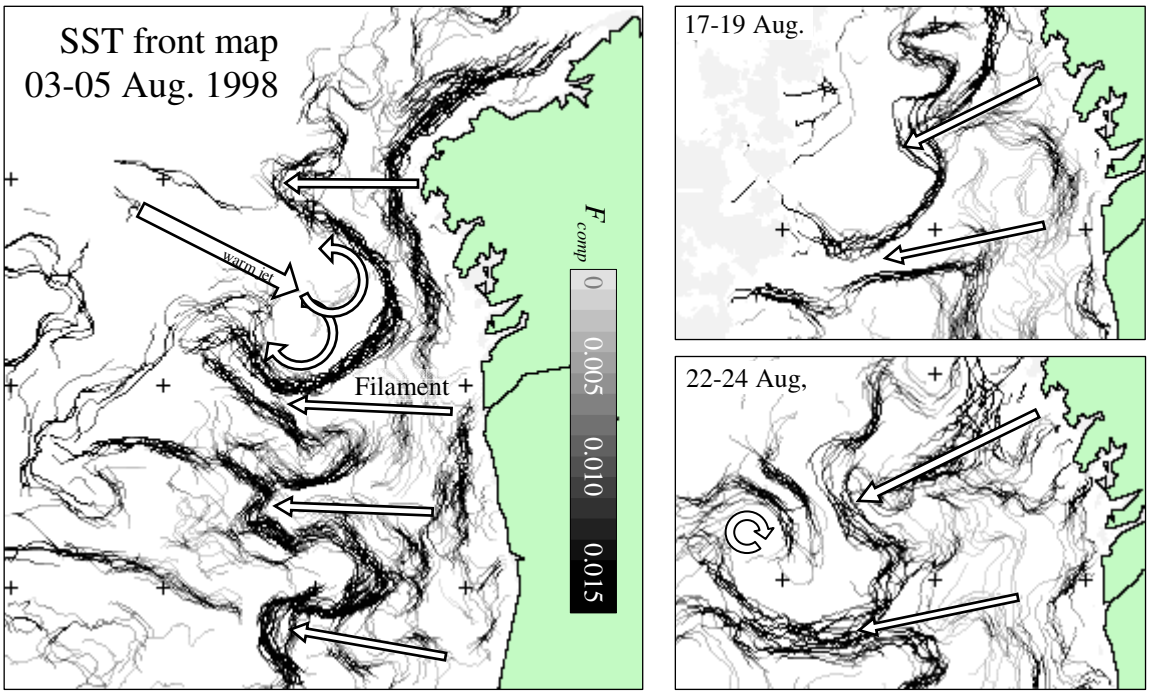

(a) *(b)*

Figure 5. Upwelling and filaments at the NW Iberian Peninsula: (a) SST front map 3-5 Aug. 1998 with filaments, a warm jet and eddies indicated by arrows; (b) SST front maps for 17-19 and 22-24 Aug. 1998 showing dynamic growth of new filament.

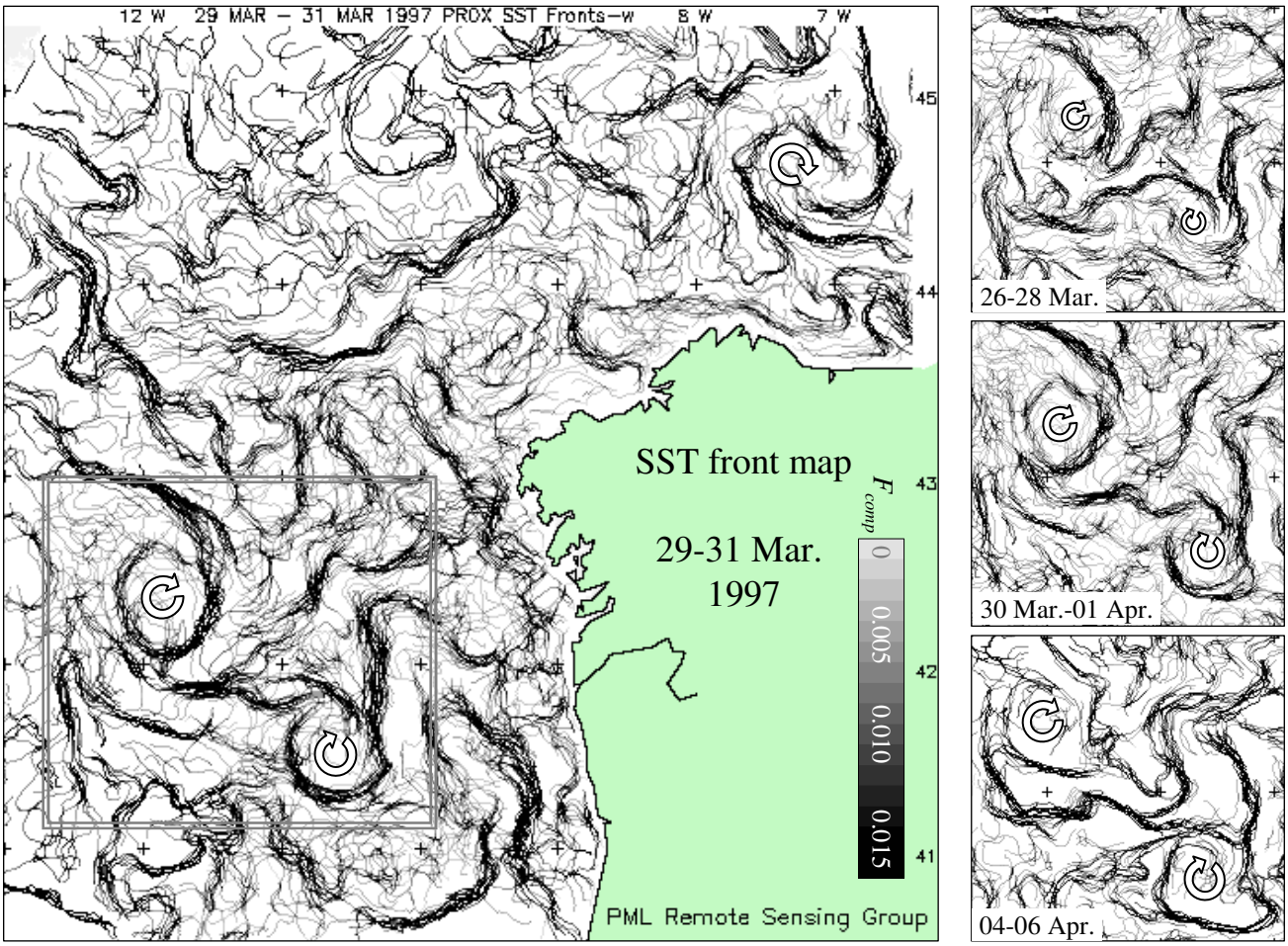

(a) *(b)*

Figure 6. Mesoscale eddies at the NW Iberian Peninsula: (a) SST front map 29-31 Mar. 1997 with several eddies indicated by arrows; (b) Sequence of SST front maps during Mar.-Apr. 1997 showing rotation, advection and distortion of two eddies, region indicated by rectangle in main figure.

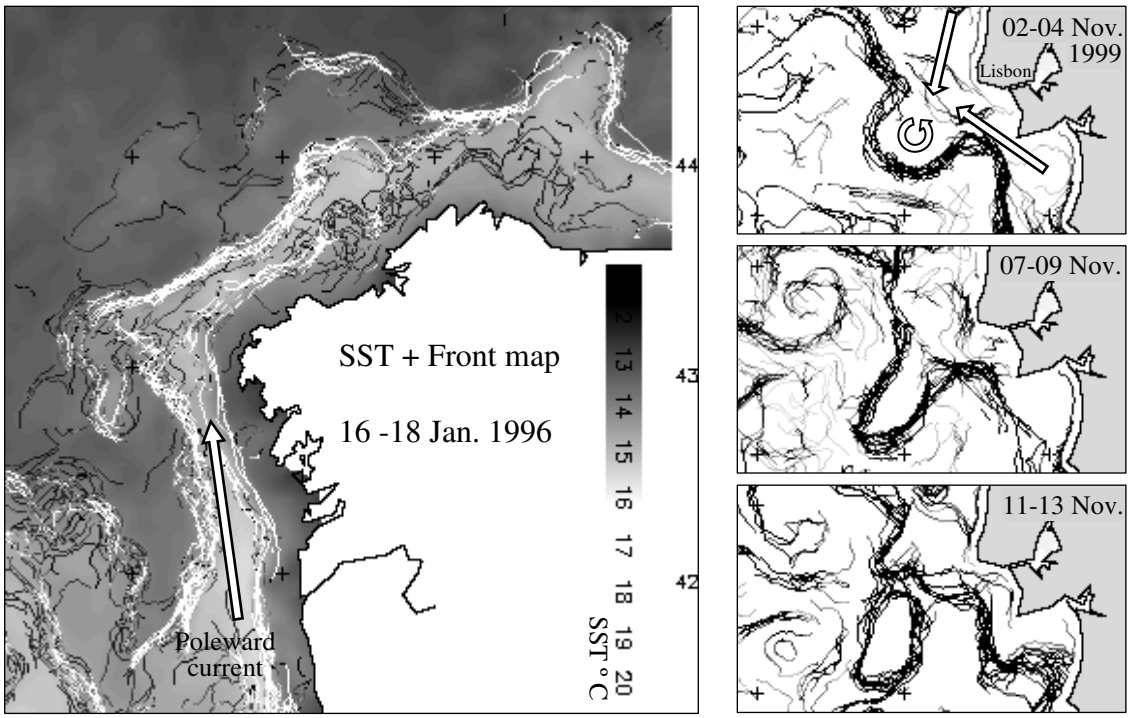

(a) *(b)*

Figure 7. Poleward flow at the NW Iberian Peninsula: (a) SST front map 16-18 Jan. 1996 showing winter poleward flow of warm water at the surface; (b) Sequence of SST front maps from Nov. 1999 showing a cyclonic eddy detaching from shelf-edge near Lisbon.